Form birefringence of anisotropically nanostructured silicon

N. Künzner, J. Diener, E. Gross, and D. Kovalev
Physik Department, Technische Universität München, D-85747 Garching, Germany

V. Yu. Timoshenko
Physics Department, Moscow State M. V. Lomonosov University, 119992 Moscow, Russia

M. Fujii
Department of Electrical and Electronics Engineering, Faculty of Engineering, Kobe University, Rokkodai, Nada, Kobe 657-8501, Japan

(Received 12 July 2004; revised manuscript received 12 November 2004; published 4 May 2005)

We present a detailed study of the anisotropic optical properties of mesoporous silicon layers prepared from substrates having different doping levels under various preparation conditions. We demonstrate that the morphology of the layers strongly depends on the preparation conditions. It correlates with measured optical anisotropy values and defines the directions of the optical axes. The experimental data are explained in the framework of an effective medium model which takes into account the different morphologies of the layers. Modifications of the optical anisotropy of the layers in a controlled manner by filling the pores with dielectric substances and by oxidation of the structure confirm that form birefringence is the origin of the optical anisotropy.

DOI: 10.1103/PhysRevB.71.195304 PACS number(s): 78.55.Mb, 78.66.−w

I. INTRODUCTION

Nanostructuring is a fast growing field in modern solid-state physics. Among other techniques it enables to overcome restrictions entailed with the natural (bulk) materials via tuning their physical properties as desired for applications. As an example we refer to photonic crystals, artificially created structures consisting of spatially ordered well-defined fragments having sizes comparable to the wavelength of near-infrared light.[1,2] A strong wavelength-dependent scattering of light leads to the appearance of photonic bandgaps. But even when the wavelength of light (λ) is much longer than the constituents (size $\approx a$) of a photonic system the propagation of light can be noticeably influenced. Two scenaria can be distinguished: either the constituents exhibit an intrinsic optical anisotropy or optically isotropic constituents are arranged spatially anisotropic (examples are bulk materials assembled by elongated molecules[3] or atoms in a noncubic lattice,[4] respectively). When $\lambda \gg a$ it is not possible to distinguish between the scenaria mentioned above for composite materials.

Recently we have shown that mesoporous silicon (*P*Si), a spongelike network of nanometer-sized pores and silicon (Si) wires, can exhibit an enormously large in-plane optical anisotropy in the visible and infrared spectral range.[5–7] We concluded that the texture of layers prepared from (110) Si substrate supports form birefringence as the origin of the optical anisotropy.[6] The optical anisotropy parameters of bulk systems are fixed. The advantage of the *P*Si layers is that these parameters can be adjusted to a desirable level via modification of their morphology. It is well known that their morphology strongly depends on the doping level of the bulk Si substrate as well as the etching current density (for a given electrolyte). However, up to now no systematic studies on the correlation of the optical anisotropy with the morphology of the *P*Si layers and the directions of the optical axes has been performed. Our purpose in this paper is to present a systematic study of these issues. We demonstrate that the birefringence level can be continuously tuned up to 0.25 via a proper choice of the etching current density and doping level of the substrate. The paper is structured as follows: in Sec. II we deal with the preparation of the *P*Si layers and the experimental techniques used. In Sec. III the morphology of the *P*Si layers and their optical properties are presented. The experimental results are discussed in Sec. IV. Finally, Sec. V contains an investigation of the optical anisotropy modified by incorporation of dielectric substances into the pores of the layers and a comparison of the experimental results with effective medium approximation (EMA) calculations.

II. EXPERIMENT

The *P*Si layers were prepared by electrochemical anodic etching of boron-doped (110) oriented bulk Si wafers having specific resistivity 30–70 mΩ cm [in the following denoted as p^+ (110) *P*Si layer] and 1–5 mΩ cm [p^{++} (110) *P*Si layer], respectively. The etching solution was a 1:1 (by volume) mixture of hydrofluoric acid (49 wt.% in water) and ethanol. Free-standing layers were obtained by an electropolishing step at the end of the etching procedure. Further details of the preparation procedure can be found elsewhere.[8] The thickness of the layers was determined using an optical microscope. Various etching current densities (10–100 mA/cm^2) were employed to obtain a wide range of porosities ($\approx$50–70% for p^+ layers and $\approx$65–80% for p^{++} layers, respectively). The orientation of crystallographic directions in the plane of the layer surface was determined by X-ray diffraction analysis. For the imaging of remnant Si

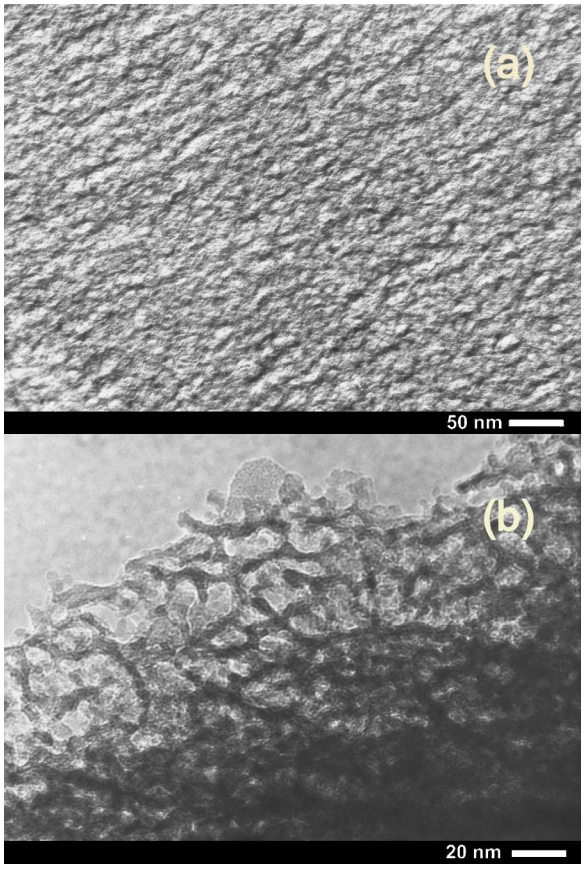

FIG. 1. (a) TEM image of the (110) surface of a p^{++}-*P*Si layer. Bottom left to top right corresponds to the $[\bar{1}10]$ crystallographic direction. (b) The TEM image of the (110) surface of a p^{+}-*P*Si layer.

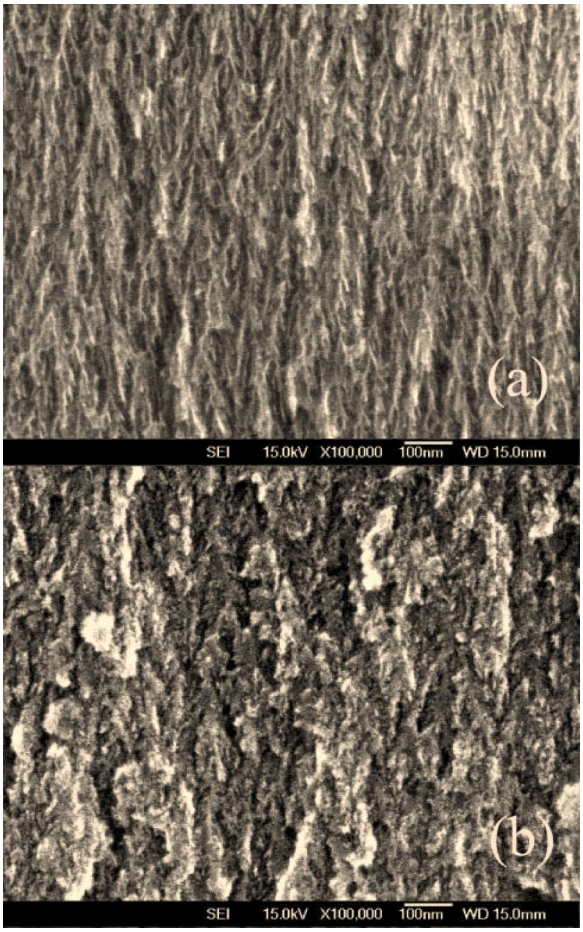

FIG. 2. (a) SEM image of a $(1\bar{1}2)$ plane of a p^{++}-*P*Si layer prepared from a (110) oriented Si substrate. (b) SEM image of a $(1\bar{1}2)$ plane of a p^{+}-*P*Si layer prepared from a (110) oriented Si substrate.

fragments and pores, a TEM setup having atomic resolution and a high resolution SEM setup have been used. Polarization-sensitive transmittance and reflectance measurements in the visible and near-infrared range (400–2000 nm) have been performed utilizing collimated white light or laser beams. Glan-Thomson prisms have been used as polarizing elements. The detection unit was either a single monochromator followed by a Si charge-coupled device or a Ge photodiode. The layers were mounted on a rotation stage in a chamber which can be evacuated or connected to a reservoir of various vapors. Vapor pressures were adjusted and controlled by a microvalve and a membrane pressure gauge. Measurements in the mid-infrared range ($\lambda > 2$ μm) were performed with a Bomem FTIR spectrometer. Infrared light was polarized by a wire-grid polarizer. The spectral response of the experimental setup was taken into account in the spectra recorded.

III. STRUCTURAL AND OPTICAL PROPERTIES

In order to correlate optical and structural properties of the (110) *P*Si layers, we start with an inspection of their microscopic structure. Figure 1 shows TEM micrographs of the (110) surface plane of a p^{++} (a) and a p^{+} (b) layer, respectively. For the p^{++} layer a macroscopic anisotropic alignment of the Si nanowires (dark) and pores (bright) from the bottom left to the upper right along the $[1\bar{1}0]$ crystallographic direction is clearly seen. For the p^{+} layer the wires tend to branch more randomly but a partial alignment of nanowires and pores can be identified. In Fig. 2, SEM micrographs obtained from the cleaved edge ((112) plane) of a p^{++} (a) and p^{+} (b) layer, respectively, are presented. In the p^{++} layer nanowires (bright) are elongated from the upper right to the bottom left and the upper left to the bottom right. The morphology of the p^{+} layer appears to be randomized and a preferential alignment of nanowires and pores is difficult to identify. In general, the sizes of pores and nanowires found in the TEM/SEM images are comparable with those in layers prepared from (100) oriented bulk Si but their spatial alignment differs.[9,10] For (100) *P*Si layers Si nanowires and pores are elongated perpendicular to the surface plane ([001] crystallographic direction) and no anisotropic alignment can be observed in the surface plane. During the electrochemical etching process pores grow preferentially in ⟨100⟩ crystallographic directions due to the better polarizability of Si-H bonds on the (100) Si surfaces. For (110) Si surfaces pores are growing preferentially in the [010] and [100] crystallographic directions and their projection on the surface plane

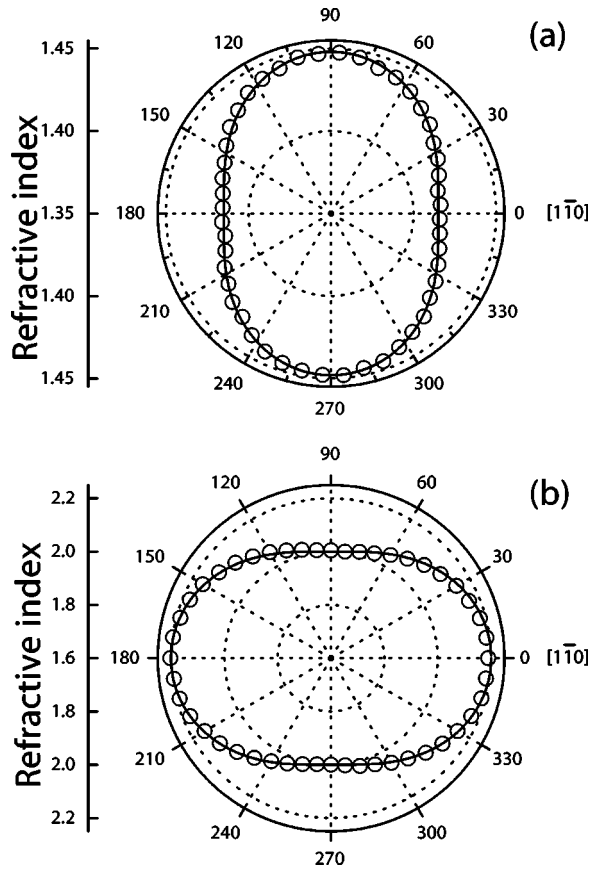

FIG. 3. Angular dependence of the refractive index of a p^+- (a) and p^{++}- (b) *P*Si layers obtained from reflectivity measurements of linearly polarized light. The polarization direction of a linearly polarized Ar^+-ion laser beam ($\lambda = 514$ nm) has been rotated around an axis perpendicular to the layer surface. The zero degree corresponds to the in-plane $[1\bar{1}0]$ crystallographic direction. Solid lines are results of a fit.

results in an overall alignment in the $[1\bar{1}0]$ crystallographic direction, as seen in Fig. 1(a).

The anisotropic morphology of these *P*Si layers results in their anisotropic optical properties.[5,6] Since the sizes of the Si nanowires and pores are significantly smaller than the wavelength of visible and infrared light standard spectroscopic techniques can be employed to characterize the optical properties of the layers. First of all, the reflectivity of linear polarized light under normal incidence of (110) p^+ and p^{++} layers has been measured as a function of the in-plane polarization direction. The refractive indices shown in Fig. 3 exhibit a strong dependence on the polarization direction of the linearly polarized light. The patterns can be properly described by assuming uniaxial in-plane birefringence of the *P*Si layers (Fig. 3, solid line).

According to Fig. 3 the refractive indices of the p^{++} layer $n_{[1\bar{1}0]} = 2.20$ and $n_{[001]} = 2.0$ were extracted, where $n_{[1\bar{1}0]}$, $n_{[001]}$ are the refractive indices for light polarized along the orthogonal in-plane crystallographic directions $[1\bar{1}0]$ and $[001]$, respectively. For the p^+ layer the refractive indices are found to be $n_{[1\bar{1}0]} = 1.42$ and $n_{[001]} = 1.45$. Note that the birefringence $\Delta n = |n_{[1\bar{1}0]} - n_{[001]}|$ is smaller for the p^+ layer and

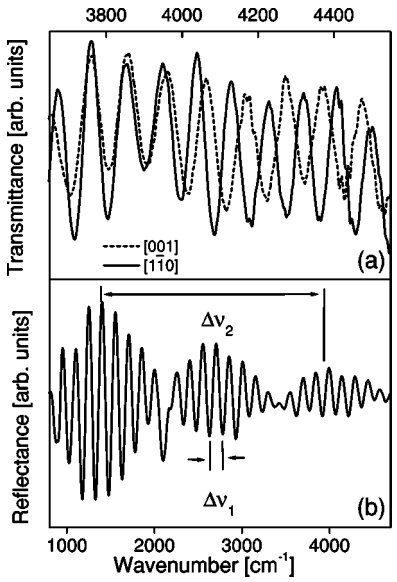

FIG. 4. (a) Transmittance spectrum of a p^{++} (110) *P*Si layer for linearly polarized infrared light. (b) Reflectance spectrum of a p^{++} (110) *P*Si layer for randomly polarized incident light.

that the optical anisotropy is reversed for p^{++} and p^+ layers. The value of the mean refractive index $\bar{n} = (n_{[1\bar{1}0]} + n_{[001]})/2$ is in agreement with the measured isotropic in-plane refractive index for mesoporous Si samples prepared from (100) bulk Si having comparable porosities.[11] For light polarized along one of the principal in-plane refractive index axes ($[1\bar{1}0]$, $[001]$) no change of the polarization state of the transmitted light is observed.

We extend the investigation of the birefringence of *P*Si layers to the infrared spectral range when the photon energy is far below the value of the bandgap of bulk Si. Figure 4(a) shows the spectrum of infrared light polarized either along the $[1\bar{1}0]$ or $[001]$ crystallographic direction transmitted through a p^{++} (110) *P*Si layer. Well-pronounced interference fringes arising from multiple reflections indicate that the thickness of the layer is homogeneous. The spacing between the fringes depends on the polarization direction of the incident light. It is smaller for the polarization in the $[1\bar{1}0]$ direction. This evidences the larger value of the refractive index. For p^+ (110) *P*Si layers the refractive index is larger for light polarized along the $[001]$ crystallographic direction. Employing unpolarized light, the optical properties of a *P*Si layer are averaged over all polarization directions. In Fig. 4(b) the reflectance spectrum of a p^{++} (110) *P*Si layer for randomly polarized infrared radiation is shown. Randomly polarized light has two components polarized along the $[1\bar{1}0]$ and $[001]$ directions and their interference results in a characteristic beat structure. A quantitative analysis of the spectrum allows us to estimate both the average refractive index $\bar{n} = 1.68$ from the oscillations having small spacing ($\Delta\nu_1$) as well as the birefringence $\Delta n = 0.19$ from the envelope function of the beats ($\Delta\nu_2$).

Experiments under normal incidence do not allow to deduce the exact symmetry of the birefringent layers because they can be uniaxial or biaxial as well as negative or posi-

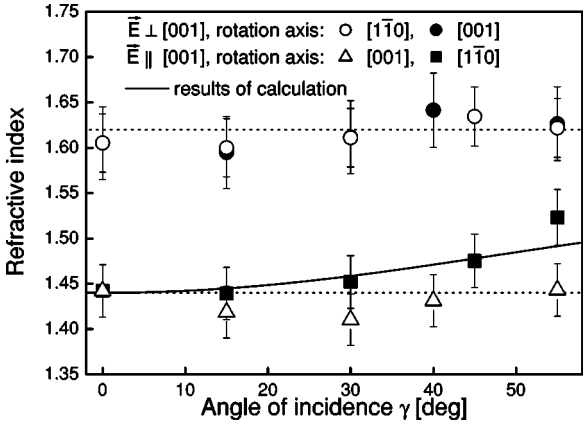

FIG. 5. Dependencies of refractive index values for a p^{++}-*P*Si layer on the angle of incidence of infrared radiation (400–4000 cm^{-1}) polarized along [001] and [1$\bar{1}$0], respectively. Error bars result from uncertainties in the layer thickness and the angle of incidence. A solid line shows the result of calculations.

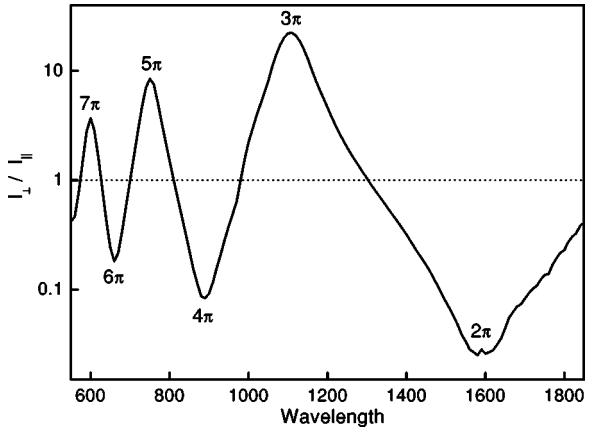

FIG. 6. $I_\perp/I_\parallel$ obtained for a p^{++}-*P*Si layer (j=30 mA/cm^2) prepared from a (110) Si substrate. Phase shifts are related to the maxima and minima are indicated.

tive. To clarify the symmetry of birefringent layers, angular-resolved transmission measurements with polarized infrared light were performed. Transmission spectra of infrared light for the sample rotated around either the [001] or the [1$\bar{1}$0] axis have been measured. The incident light was polarized either along [001] or [1$\bar{1}$0] (crystallographic directions for normal incidence). The refractive index obtained for light polarized perpendicular to the optical axis of a uniaxial layer is constant while the layer is rotated around the optical axis (ordinary beam). However, light polarized in the plane spanned by the optical axis and the wave vector experiences a refractive index given by Eq. (1),[12]

$$n(\theta) = \frac{n_{[1\bar{1}0]} n_{[001]}}{\sqrt{n^2_{[1\bar{1}0]} \sin^2\theta + n^2_{[001]} \cos^2\theta}}; \qquad (1)$$

θ denotes the angle between the optical axis and the propagation direction inside of the layer and [001] is assumed to be the optical axis. The rotation of a p^{++} layer around the [1$\bar{1}$0] axis affects the refractive index only when the incident light is polarized along [001] while in all other geometries the refractive index is insensitive to the angle of incidence γ (see Fig. 5). Therefore the optical axis can be assigned to the [001] crystallographic direction. The solid line in Fig. 5 represents a corresponding calculation where θ was recalculated from γ according to Snells law. The measured dependence of $n(\gamma)$ coincides with calculations what confirms the optical uniaxiality of the p^{++} layers. For a p^+ sample the small birefringence Δn complicates quantitative analysis of the angular dependence of the refractive index values. Therefore these measurements can be performed accurately only for large angles of incidence. The maximal variation of the refractive index has been found to be on the order of 0.01. We conclude that it is also optically uniaxial and the direction of the optical axis is [1$\bar{1}$0]. Thus, both layers exhibit the optical properties of negative uniaxial birefringent crystals.

To define the anisotropy parameters in a wide spectral range, the layers were placed between two polarizing elements and the light was incident normal to the surface. The polarization direction of the incident light was oriented 45 ` to the [1$\bar{1}$0] and [001] axes, respectively. For each layer, two transmission spectra have been recorded: $I_\perp$ for crossed and $I_\parallel$ for parallel polarization directions of the polarizer and the analyzer, respectively. From the ratio $I_\perp/I_\parallel$ for a flat birefringent layer having uniform thickness d, the spectral dispersion of Δn can be extracted according to Eq. (2),

$$\frac{I_\perp}{I}(\lambda) = \frac{\sin^2\left(\frac{2\pi}{\lambda} d \frac{\Delta n}{2}\right)}{\cos^2\left(\frac{2\pi}{\lambda} d \frac{\Delta n}{2}\right)}. \qquad (2)$$

In Fig. 6 the ratio $I_\perp/I_\parallel$ for a p^{++} layer is shown. The function is oscillating but poles expected when the denominator in Eq. (2) equals zero are absent. This fact and the decreasing amplitude for smaller wavelengths can be attributed to a small thickness nonuniformity of the layer.

While light travels through the optically anisotropic layer its components polarized along [001] and [1$\bar{1}$0] directions experience a phase shift $\Delta\phi$. According to Eq. (2) the maxima in the $I_\perp/I_\parallel$ curve correspond to odd, minima to even orders of π. The phase-shifts are indicated in Fig. 6. According to the relation $\Delta n = (\lambda/2\pi)(1/d)\Delta\phi$, the anisotropy parameter can be determined. λ denotes the wavelength of the maximum or minimum corresponding to the phase shift $\Delta\phi$. For smaller wavelengths the spectral spacing of maxima and minima in $I_\perp/I_\parallel$ becomes smaller and their spectral positions become redshifted due to the spectral dispersion of Δn.

IV. DISCUSSION

At this point we want to discuss the origin of birefringence in solids and specify the mechanism of birefringence in *P*Si layers on the basis of the results presented until now.

Later our conclusions will be supported by additional experiments. In bulk crystals birefringence is governed by a background (Penn gap) and a resonant electronic contribution. The anisotropic arrangement of atoms in the unit-cell of $A_{II}-B_{VI}$ compounds induces a splitting of the hh-lh bands. Their coupling strength to linearly polarized light is different which leads to a resonant contribution to birefringence most efficient at the band gap. Si having a highly symmetric diamond-type unit cell (T_d symmetry) is optically isotropic. Only a small birefringence on the order of 10^{-5} is observed due to spatial dispersion effects.[13] Additionally, in bulk crystals birefringence can be induced by application of external stress. According to X-ray analysis nanowires in *P*Si layers possess the diamondlike lattice structure of bulk Si. Simple estimates based on elasto-optic constants show that the birefringence induced by the distortion of the crystalline lattice structure on the surface of the nanowires is negligibly small.[14] The crystalline structure of Si nanowires is therefore believed to be optically isotropic.

In 1904, Braun suggested that birefringence can be achieved in a composite system by an anisotropic spatial arrangement of its optically isotropic constituents.[15] This effect is referred as form birefringence and anisotropic optical properties of the system arise from polarization-dependent screening induced by the electric field of the propagating light wave. Form birefringence was found to play an important role in the optical properties of nanostructures, e.g., stacks of semiconductor layers.[16] Particularly in this case an additional contribution to birefringence caused by polarization-dependent selection rules for electronic quantum confined states is present. For a composite structure local field effects have to be taken into account. However, the sizes of nanowires in mesoporous Si layers suggest that quantum confinement effects can be neglected here. The indirect nature of optical transitions in Si in the vicinity of the fundamental band edge and consequentially the small oscillator strength rule out a contribution to birefringence caused by polarization-dependent optical transitions in the spectral range investigated. To confirm that form birefringence is the origin of optical anisotropy of (110) *P*Si layers we investigated how the spatial alignment of the microstructure affects the anisotropy parameter Δn. The morphology of *P*Si layers can be changed either by varying the doping level of the Si substrate or the etching current density. The mean size and spatial alignment of remnant Si nanocrystals depend strongly on the doping level of the Si substrate used.[10] Figure 7 shows the spectral dispersion of the anisotropy parameter for p^+ and p^{++} *P*Si layers. Over the whole spectral range the anisotropy parameter is substantially larger for the p^{++} layer. This agrees with the anisotropic alignment of Si nanowires in the (110) layer surface plane shown in the TEM image of Fig. 1. The level of alignment of Si nanowires is significantly larger for p^{++} layers which correlates with the birefringence Δn. Next, in Fig. 8 the spectral dispersion of Δn for different etching current densities used to form p^{++} (a) and p^+ (b) layers is compared. The dependence for p^{++} and p^+ layers is opposite. For p^{++} layers the birefringence increases with etching current density while it decreases for p^+ layers. It should be noted that even for the highest current density used for p^+ and the lowest for p^{++} layers, Δn is still three times larger for p^{++} layers.

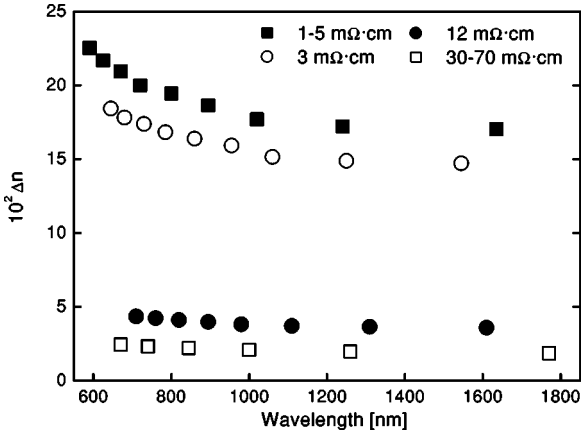

FIG. 7. Spectral dependence of the anisotropy parameter Δn of *P*Si layers prepared from substrates having different doping levels. All layers have been prepared with equal etching current densities ($j=50$ mA/cm^2).

The dissolution of Si is promoted by a weakening of hydrogen-passivated Si bonds by fluorine atoms. The morphology of *P*Si layers is determined by the anisotropic pore growth and the stability of pore walls. Hydrogen passivation is most efficient for {111} surfaces having the smallest amount of Si dangling bonds. It has been demonstrated for a variety of Si substrates, that pore growth proceeds preferentially along ⟨100⟩ and, to smaller extent, ⟨113⟩ directions.[17]

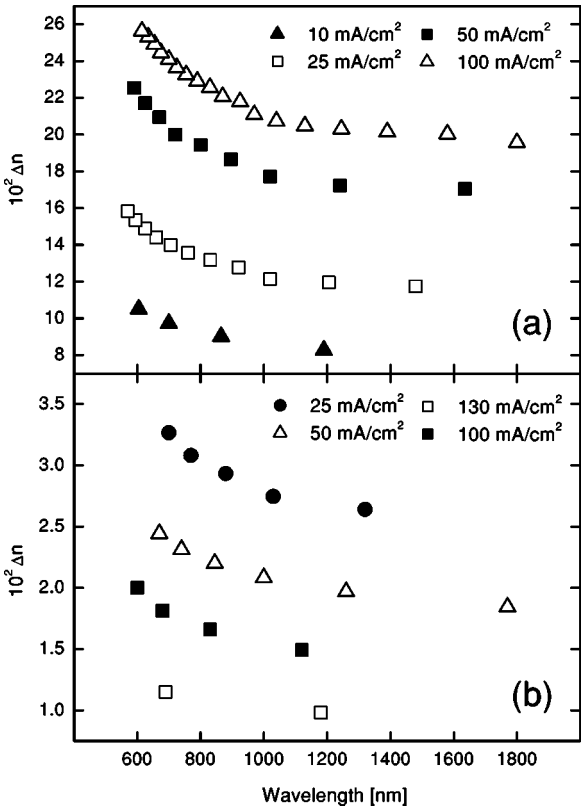

FIG. 8. Spectral dependence of the anisotropy parameter Δn of p^{++}- (a) and p^+- (b) *P*Si layers prepared from a (110) Si substrate with different etching current densities.

For {100} and {113} surfaces the saturation of the dangling bonds is comparably slow what results in pore propagation perpendicular to these planes.

For (110) oriented Si substrate the preferential pore growth is along [100] and $[0\bar{1}0]$ directions aligned 45 ° to the surface with projection $[1\bar{1}0]$ in the surface plane. Perpendicular to that pore growth proceeds in the [001] direction lying in the surface plane. This consideration explains the characteristic anisotropic morphology shown in Fig. 1 with nanowires aligned along $[1\bar{1}0]$. The structure sizes of the nanowires and pores in *P*Si layers are determined also by the doping level of the substrate influencing the thickness of the space-charge region in remnant Si fragments. In the p^+ substrate the morphology is determined by pore wall passivation controlled by the formation of a charge carrier depletion layer. The holes are diffusively driven through the depletion layer by the electric field having its highest value at the pore tips, resulting in narrow pores. When further hole diffusion is blocked by the repulsive local electric field of a charged dopant atom the pore growth is guided to another preferential growth direction. The frequent changes of pore growth directions reduce the level of morphological and, therefore, optical anisotropy. Increased etching current densities lead to a more isotropic morphology with the subsequent reduction of optical anisotropy. For heavily doped p^{++} substrates the pore growth proceeds via tunneling of holes through the extremely narrow space-charge region. Pore diameters are larger in this regime since the electric field required to inject the holes through the depletion layer is small. Thus, *P*Si layers prepared from p^{++} substrates possess an extended morphological and, therefore, optical anisotropy. Furthermore, an increase of Δn for larger current densities can be explained by a better alignment of Si nanowires and pores along the preferential pore growth directions.

V. THEORY AND MODEL

Form birefringence is a well-known phenomenon and has been successfully described theoretically. We would like to model the optical anisotropy of the *P*Si layers and compare model predictions with experimental results. By means of an effective medium approach a composite systems having heterogeneous microscopic structure is transformed into a homogeneous anisotropic medium featuring effective physical properties. To describe the optical properties of *P*Si layers we employed the Bruggeman effective-medium model (EMA).[18] The mean sizes of Si nanowires and pores inside our mesoporous Si layers are in the range $\approx 5-50$ nm and are therefore significantly smaller than the wavelength of light used to probe the layers. Thus, the conditions for applicability of the EMA (static electric field model) are fulfilled. The *P*Si layers contain anisotropically aligned nanowires and pores and the original isotropic EMA has to be extended to account for polarization-dependent depolarization effects resulting in a tensorial character of the dielectric function.[19] We consider the *P*Si layers as a system of dielectric ellipsoids having refractive index n_{Si} and n_P representing the nanowires and pores, respectively. The anisotropic polarizability of the ellipsoids has been taken into account using different depolarization factors $L_{1,2,3}$ for the ellipsoids main axes. The uniaxiality of the (110) *P*Si layers is modeled by dielectric ellipsoids which possess rotational symmetry with their symmetry axes aligned in a single direction. Further, for simplicity it is assumed that all ellipsoids have the same depolarization factors. In general, the depolarization factors fulfill the relation $\Sigma_{i=1,2,3} L_i = 1$. To account for the negative uniaxiality of p^{++} and p^+ layers, their depolarization parameters are assumed to be $L_{[1\bar{1}0]} = 1 - 2 \cdot L_{[001]}$ and $L_{[001]} = 1 - 2 \cdot L_{[1\bar{1}0]}$, respectively.[20] For the generalized EMA the following equations have to be solved for the refractive index n dependent on the polarization direction of the external electric field:[20]

$$(1-P) \cdot \frac{n_{\mathrm{Si}}^2(\lambda) - n_{[1\bar{1}0],[001]}^2}{n_{[1\bar{1}0],[001]}^2 + L_{[1\bar{1}0],[001]} \cdot \left[n_{\mathrm{Si}}^2(\lambda) - n_{[1\bar{1}0],[001]}^2 \right]} + P \cdot \frac{n_P^2 - n_{[1\bar{1}0],[001]}^2}{n_{[1\bar{1}0],[001]}^2 + L_{[1\bar{1}0],[001]} \cdot \left[n_P^2 - n_{[1\bar{1}0],[001]}^2 \right]} = 0. \tag{3}$$

Subscripts denote the polarization directions of the incident light and P is the porosity of the layer. Note, that the spectral dispersion of the refractive index of bulk Si $n_{\mathrm{Si}}(\lambda)$ is taken into account. The spectral dependence of $\Delta n_{[001],[1\bar{1}0]}$ for *P*Si layers prepared from substrates having different doping levels and etching current densities is obtained using only one parameter (the depolarization factor L) to achieve the best fit to the experimental data. The straight lines in Fig. 9 display the spectral dispersion of Δn calculated for a p^{++} layer ($P = 73\%, L = 0.43$) and a p^+ layer ($P = 63\%, L = 0.34$). Both the birefringence values and their spectral dispersion can be described successfully by the EMA. While the birefringence values depend on the morphology of the layers their spectral dispersion is completely governed by the spectral dispersion of the refractive index of bulk Si.

This indicates that other contributions to the optical anisotropy different from form birefringence, e.g., polarization-dependent optical transition matrix elements, are either absent or negligibly small. The constant anisotropy parameter Δn in the infrared spectral region and its rise towards shorter wavelengths can be fully attributed to the spectral dispersion of the refractive index of bulk Si. Below the indirect bandgap n_{Si} is constant. Above the bandgap it rises very slowly due to the small oscillator strength of the indirect transition and the fact that the photon energy is still far below the direct bandgap.

We performed additional experiments to support the EMA model describing the optical anisotropy of *P*Si layers. The incorporation of a dielectric substance having a refractive index smaller than bulk Si into the pores of *P*Si layers reduces their optical anisotropy (e.g., a resubstitution of the pores with Si would result in the original optically isotropic bulk Si).[21] Thus, a parameter in Eq. (3), namely the refractive index of the pores, can be modified in a controlled manner. The pores of p^{++} and p^+ layers were filled with various

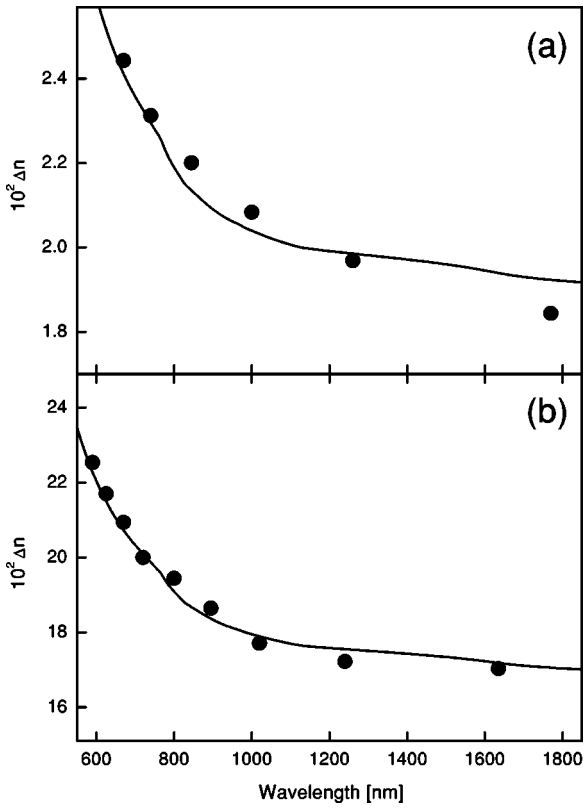

FIG. 9. A comparison of the spectral dependence of Δn for a p^+- (a) and a p^{++}- (b) *P*Si layer with the results of calculations according to the Bruggeman EMA (solid lines).

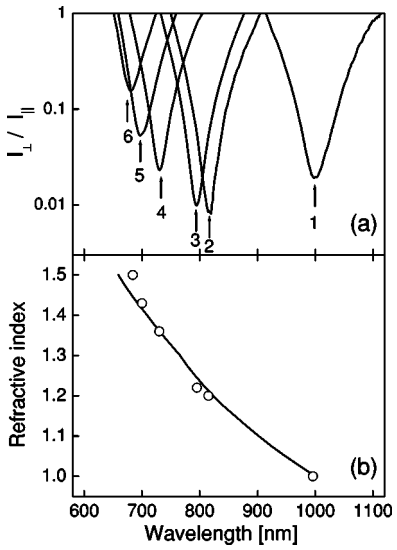

FIG. 10. (a) Shift of the minimum ($\Delta\phi=4\pi$) in the $I_\perp/I_\parallel$ curve after filling of the pores by different dielectric substances. 1—empty pores; 2—liquid nitrogen ($n=1.2$); 3—liquid argon ($n=1.22$), 4—acetone ($n=1.36$); 5—cyclohexane ($n=1.43$); and 6—benzene ($n=1.5$). (b) A comparison of the spectral shift shown in (a) with the result of a calculation according to the Bruggeman EMA (solid line).

dielectric substances (liquid nitrogen and argon, acetone, cyclohexane, and benzene having refractive indices 1.2, 1.22, 1.36, 1.43, 1.5, respectively) and for each case the transmission spectrum $I_\parallel$ and $I_\perp$ was determined. Due to the reduced optical anisotropy the phase shifts $\Delta\phi$ appear at shorter wavelengths and the $I_\perp/I_\parallel$ curve is blue-shifted. The blue-shift of $I_\perp/I_\parallel$ for a p^{++} layer was so large that it fell in the strong absorption range of the *P*Si layers. In Fig. 10 we present $I_\perp/I_\parallel$ for a p^+ layer filled by various dielectric substances. For larger values of the refractive index of the incorporated substance the blue-shift of a certain maximum or minimum corresponding to a phase shift $\Delta\phi$ is larger. To test EMA predictions we first fitted the spectral dependence of $\Delta n(\lambda)$ for the layer in air. Then the refractive index of the pores was replaced by the refractive index of the liquids. The spectral position of the minimum having $\Delta\phi=4\pi$ was calculated with the EMA [the solid line in Fig. 10(b)]. A good agreement between measured values (open circles) and predictions of EMA is clearly seen.

For porous silicon another variable parameter is the refractive index of wires assembling the layers. Thermal annealing of p^+ and p^{++} layers at 950 °C for 1 min in air transforms Si nanowires to SiO_2 wires having a constant refractive index $n_{SiO_2}\approx 1.5$ in the visible and near-infrared spectral range. After the annealing the layers appear to be completely transparent, i.e., are converted into porous quartz. Δn for the oxidized p^{++} layer is ≈ 0.02. For the p^+ layer, Δn is negligibly small. The substantially smaller optical anisotropy can be accounted to the smaller refractive index of SiO_2 compared to Si. EMA calculations predict a reduction of Δn for the p^{++} layer by a factor of 15, which is in good agreement with the determined value. Since the expansion of SiO_2 wires during the oxidation can change their shapes, a more detailed quantitative analysis is difficult.

VI. SUMMARY

We presented a comprehensive study of the morphology and anisotropic optical properties of mesoporous Si prepared from (110) bulk Si wafers. We found a strong correlation between the morphology of the layers and the optical anisotropy. This indicates a form birefringence nature of the observed effect. Values of the in-plane birefringence of the mesoporous Si layers depend on the doping level of Si substrates and the etching current densities and can be continuously tuned up to 0.25. The mesoporous Si samples exhibit the properties of a negative optically uniaxial birefringent crystal while the direction of the optical axes depends on the doping level of the substrate. These observations are discussed in detail and form birefringence is experimentally verified by reducing the optical anisotropy via either the incorporation of various dielectric substances into the pores or by oxidation of the layers. The possibility of fine-tuning of the birefringence level gives an opportunity to employ mesoporous Si layers as a phase-matching matrix for nonlinear wave interactions with active media having normal dispersion of the dielectric function embedded in the pores.

ACKNOWLEDGMENTS

This work was partially supported by CRDF Grant No. RE2-2369, the Russian Foundation for Basic Research (Grant No. 04-02-08083), the Volkswagen Foundation (Project I/76 869), and the Deutsche Forschungsgemeinschaft DFG (Project Ko 1966/3-1). V.Yu.T. and M.F. are grateful to the Alexander von Humboldt Foundation.

[1] S. W. Leonard, H. M. van Driel, K. Busch, S. John, A. Birner, A.-P. Li, F. Müller, U. Gösele, and V. Lehmann, Appl. Phys. Lett. **75**, 3063 (1999).
[2] J. D. Joannopolous, R. D. Maede, and J. N. Winn, *Photonic Crystals: Molding the Flow of Light* (Princeton University Press, Princeton, NJ, 1999).
[3] W. L. Bragg and A. B. Pippard, Acta Crystallogr. **6**, 865 (1953).
[4] Consider for example atoms in a tetragonal or hexagonal crystal lattice.
[5] D. Kovalev, G. Polisski, J. Diener, H. Heckler, N. Künzner, V. Yu. Timoshenko, and F. Koch, Appl. Phys. Lett. **78**, 916 (2001).
[6] N. Künzner, D. Kovalev, J. Diener, E. Gross, V. Yu. Timoshenko, G. Polisski, F. Koch, and M. Fujii, Opt. Lett. **26**, 1265 (2001).
[7] L. A. Golovan, V. Yu. Timoshenko, A. B. Fedotov, L. P. Kuznetsova, D. A. Sidorov-Biryukov, P. K. Kashkarov, A. M. Zheltikov, D. Kovalev, N. Künzner, E. Gross, J. Diener, G. Polisski, and F. Koch, Appl. Phys. B: Lasers Opt. **73**, 31 (2001).
[8] O. Bisi, S. Ossicini, and L. Pavesi, Surf. Sci. Rep. **38**, 1 (2000).
[9] A. G. Cullis, L. T. Canham, and P. D. J. Calcott, J. Appl. Phys. **82**, 909 (1997).
[10] V. Lehmann, R. Stengl, A. Luigart, Mater. Sci. Eng., B **69-70**, 11 (2000).
[11] W. Theiß, Surf. Sci. Rep. **29**, 91 (1997).
[12] R. L. Sutherland, *Handbook of Nonlinear Optics* (Marcel Dekker, New York, 1996).
[13] J. Pastrnak and K. Vedam, Phys. Rev. B **3**, 2567 (1971).
[14] I. Mihalcescu, G. Lerondel, and R. Romestain, Thin Solid Films **297**, 245 (1997).
[15] F. Braun, Phys. Z. **8**, 199 (1904).
[16] A. A. Sirenko, P. Etchegoin, A. Fainstein, K. Eberl, and M. Cardona, Phys. Rev. B **60**, 8253 (1999).
[17] M. Christophersen, J. Carstensen, S. Rönnebeck, C. Jäger, W. Jäger, and H. Föll, J. Electrochem. Soc. **148**, E267 (2001).
[18] D. A. G. Bruggeman, Ann. Phys. **24**, 636 (1935).
[19] D. Stroud, Phys. Rev. B **12**, 3368 (1975).
[20] J. E. Spanier and I. P. Herman, Phys. Rev. B **61**, 10437 (2000).
[21] N. Künzner, E. Gross, J. Diener, D. Kovalev, V. Yu. Timoshenko, and D. Wallacher, J. Appl. Phys. **94**, 4913 (2003).